Int J Adv Manuf Technol (2018) 94:4247–4263
DOI 10.1007/s00170-017-1127-y

ORIGINAL ARTICLE

Application and analysis of spread die and flat container in the extrusion of a large-size, hollow, and flat-wide aluminum alloy profile

Dong Wang[1,2] · **Cunsheng Zhang**[1,2] · **Cuixue Wang**[2] · **Guoqun Zhao**[2] · **Liang Chen**[2] · **Wenchao Sun**[3]

Received: 27 June 2017 / Accepted: 13 September 2017 / Published online: 2 October 2017

Abstract The structure of the extrusion die has great influence on material flow balance and product quality for large-size aluminum alloy profiles, especially the preallocated structure, such as spread die and flat container. In this work, regarding the practical problems existing in practical production of a large-size, hollow, and flat-wide aluminum alloy profile used in the high-speed train, the porthole extrusion process with cylinder container and spread die is firstly simulated using HyperXtrude and verified experimentally. The spread die is then optimized by combining the design of experiments with response surface method. With the optimized spread die, the maximum velocity difference in the cross section of the profile reduces from 8.63 to 3.07 mm/s, and the corresponding SDV reduces from 1.56 to 0.69 mm/s. Finally, the different structures of containers are designed; the effects of cylinder container and flat containers with different transition form on material flow, billet skin, and die stress in numerical simulation process are comparatively analyzed; and the design rules of extrusion dies are summarized for large-size, hollow, and flat-wide aluminum alloy profiles. By comparison, the maximum velocity difference decreases from 14.41 to 3 mm/s, and the maximum stress on the extrusion dies decreases from 999 to 670 MPa, and the dead zone also greatly decreases in flat container extrusion.

Keywords Aluminum alloy profiles · Porthole extrusion die · Spread die · Flat container

✉ Cunsheng Zhang
zhangcs@sdu.edu.cn

[1] Shenzhen Research Institute of Shandong University, Shenzhen, Guangdong 518057, People's Republic of China

[2] Key Laboratory for Liquid-Solid Structural Evolution and Processing of Materials (Ministry of Education), Shandong University, Jinan, Shandong 250061, People's Republic of China

[3] Conglin Aluminum Co., Ltd., Yantai, Shandong 265705, People's Republic of China

1 Introduction

Thanks to their low density, high strength-to-weight ratio, corrosion resistance, and other good physical features, aluminum alloy profiles have been widely used in the bodies of high-speed trains, subways, and other fields. Moreover, with the increasing application of aluminum alloy profiles, they are being developed with the direction of large-size, flat-wide, thin-wall, and with complex sections. Figure 1 shows the examples of aluminum alloy profiles used for manufacturing the bodies of high-speed trains.

For producing this kind of aluminum alloy profiles, porthole extrusion dies with cylinder container are widely used in actual extrusion process, as shown in Fig. 2. The heated aluminum alloy billet undergoes successively upsetting, splitting, and welding, and the profile finally is extruded out of the bearing lands of extrusion die.

In order to balance the whole material flow velocity in die cavity and to improve the service life of extrusion die, some scholars have carried out numerical simulation of extrusion process for large-size, hollow, and flat-wide aluminum alloy profiles. Lee et al. [1] have investigated the effect of chamber shapes of porthole die in condenser tube extrusion on material flow, welding pressure, extrusion load, and mandrel deflection in non-steady states using Deform-3D. Yang et al. [2] have studied the effect of various design parameters on hot extrusion of complicated

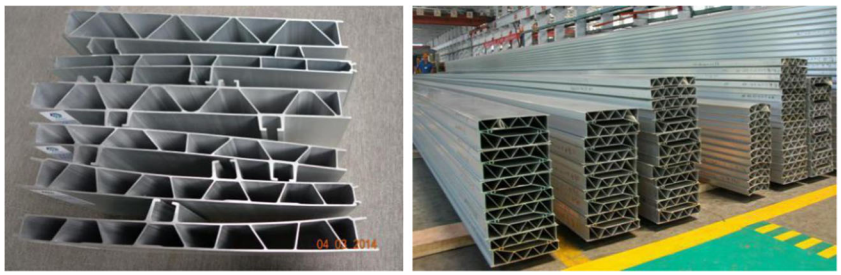

Fig. 1 Aluminum alloy profiles used in high-speed trains

aluminum alloy profiles. Liu et al. [3] have simulated the extrusion process of 6005 aluminum alloy high-speed train wallboard profile and studied the effect of resizing the portholes, adding bosses, chamfering the mandrels, and adjusting the bearings on metal flow velocity at die exit based on HyperXtrude. Zhao et al. [4] have simulated and optimized the extrusion process of a large wallboard aluminum alloy profile by adding the baffle plate and adjusting the series of the welding chamber using HyperXtrude; additionally, the results has been examined by mean of extrusion experiments. Zhang et al. [5] have optimized the layout, shapes, and heights of the baffle plate of an extrusion die to obtain the profile without the defects and verified simulated results by extrusion experiments. Sun et al. [6] have modified the height and shape of second-step welding chamber of a porthole extrusion die for high-speed train wallboard aluminum alloy profile. Reddy et al. [7] have optimized the bearing length of the extrusion die using the combination of HyperXtrude and HyperStudy. Zhang et al. [8] have automatically optimized the feeder chamber of an extrusion die with HyperMorph and HyperStudy. Mayavaram et al. [9] have adopted a new optimization algorithm about thermodynamics in extrusion process to realize the automatic optimization of the bearing length and verified the validity of the result through three examples. Bas J. E. et al. [10] have developed a numerical simulation software for analyzing the steady state extrusion process and predicting the cross-section shape of complex profile using Eulerian method.

As a typical three-dimensional deformation process, the material flow in extrusion die cavity is very complex and is difficult to control. Due to the complexity of cross-section shape, large difference of wall thickness and big ratio of width to thickness of the profile, porthole extrusion dies including multilevel porthole holes, multistep welding chambers, unequal lengths of bearing lands, and other complex structures are mainly used, which easily cause the bend or twisting deformation of profile. At the same time, the extrusion die usually works under a high temperature, high pressure, strong friction, and cyclic loading-unloading condition; as a result, the extrusion die cracks or damages easily. In order to effectively improve the uniformity of material flow and the service cycle of large-scale extrusion dies, some scholars have developed new styles of extrusion dies, such as spread die and flat container.

The spread extrusion is a new extrusion technique for producing the profiles whose width is larger than that of the container diameter. A spread die is generally added between the container and the porthole die. The cross section of the spread die is always designed as the dumb-bell shape and extended as the trumpet shape. Undergoing the predistribution and pre-deformation of the metal in spread die, the entire uniformity of material flow will be obviously improved. Sajko et al. [11] have simulated and optimized the

(a) cylinder container (b) porthole extrusion die

Fig. 2 Cylinder container and porthole extrusion die

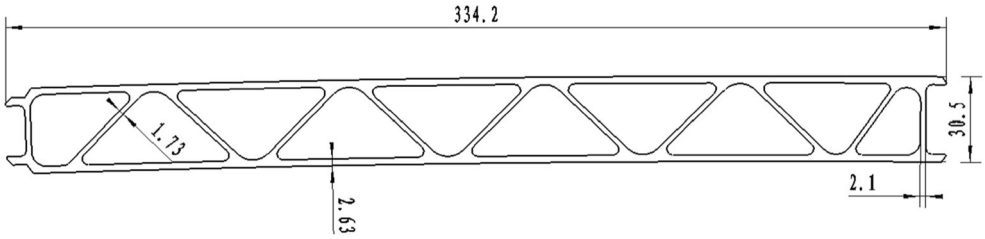

Fig. 3 Geometry and main dimensions of the aluminum alloy profile (unit: mm)

concave part of the spread die to balance the metal flow for a solid wide-flat profile by HyperXtrude. K. Abrinia et al. [12, 13] have applied the spread die during the extrusion process of a simple profile. D. Lesniak et al. [14] have compared the influence of a traditional die and a spread die on material flow velocity, surface quality, and microhardness. Fang et al. [15] have studied numerically and experimentally the effect of the die structure parameters on the solid wide-flat profile during the spread extrusion process.

The flat container extrusion is another recently developed technique for aluminum alloy profiles, especially for large-size, hollow, and wide profiles, where the flat billets are used. Because of the geometrical similarity between the flat billet and the cross-section shape of the extruded profile, the application of flat containers can improve the uniformity of material flow velocity and reduce the area of dead zone. Uniform stress distribution always occurs in flat container, which works under the high temperature, high pressure, high friction, and alternating stress, so flat containers are damaged easily compared to other cylinder containers. Therefore, the flat containers are not applied widely in the current production of large-size and flat-wide aluminum alloy profiles. American engineers firstly proposed the flat container extrusion method and applied for a relevant patent. Xu et al. [16] have analyzed the flat container using ANSYS FEM and used the pre-loaded layer with changeable shrinkage instead of the pre-loaded layer with uniform shrinkage. Some domestic scholars have researched die design, die manufacture, and structure parameter optimization of the flat container. Duan [17] optimizes the internal hole of the flat container based on analytic and numerical simulation method. Wang [18] analyzes the stress distribution and deformation of the cavity in the flat container, and puts forward some methods such as the changeable shrinking-fitting range, the gap degree, and the ellipticity.

According to the above analysis, some scholars have studied and applied the spread die or flat container during the extrusion of aluminum alloy profiles. But the current research is mainly concentrated on the solid profiles, and there is little industrial case for large, hollow, and flat-wide aluminum alloy profiles. Therefore, the purpose of this work is to investigate the material flow during the spread die extrusion and flat container extrusion for a large-size, hollow, and flat-wide aluminum alloy profile. For the spread die extrusion, a spread die will be used in the practical production and then be optimized with design of experiments and response surface method. For the flat container extrusion, the containers with different geometrical shapes will be designed and their effects on material flow, billet skin, and die stress in numerical simulation process will be comparatively analyzed. Finally, the design rules of extrusion dies will be summarized for large-size, hollow, and flat-wide aluminum alloy profiles.

2 Modeling the traditional extrusion process with a spread die

2.1 Existing problems in practical extrusion

In this study, the geometry and main dimensions of the large-size, hollow, and flat-wide aluminum alloy profile used for high-speed train are shown in Fig. 3. The profile has 10 cavities, and the cross-section area of this profile is 2451.6 mm^2. Additionally, its maximum and minimum wall thicknesses are

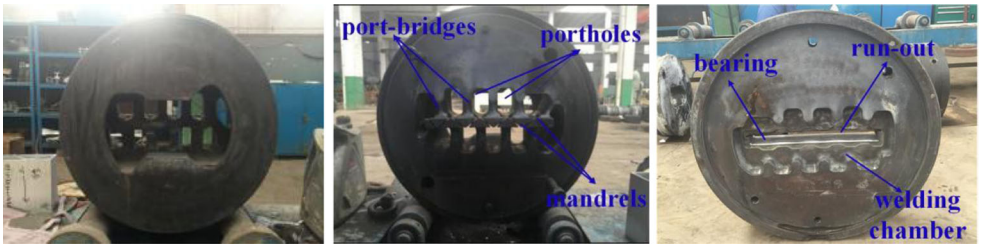

(a) spread die (b) upper die (c) low die

Fig. 4 Extrusion dies in actual extrusion process

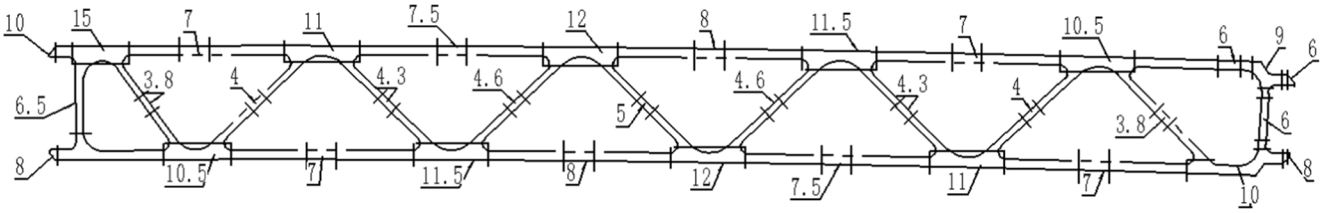

Fig. 5 Unequal lengths of the bearing lands (unit: mm)

2.63 and 1.73 mm, respectively, and the ratio of width to thickness is up to 11.

For producing this large-size, hollow, and flat-wide aluminum alloy profile, the porthole extrusion with a spread die is designed, as shown in Fig. 4. Beside upper and lower dies, a spread die is added between the upper die and the container. The spread, upper, and lower dies have the same outer diameter of 535 mm, and its heights are 120, 130, and 110 mm, respectively. The spread die is mainly used to pre-allocate material reasonably. Ten portholes are adopted in the upper die to balance material flow effectively; the lower die has specially designed two-step welding chambers. The upper and lower dies are both with unequal lengths of bearing lands to further balance material flow, as shown in Fig. 5. The design principle of the lengths of bearing lands, a long bearing land, is designed where the profile is easy to form and vice versa.

Then, the 6N01 aluminum alloy billet is extruded on an 8000-t extrusion press with the process parameters listed in Table 1. After extrusion, the front-end of the profile is obtained as shown in Fig. 6a, which is mainly used for repairing extrusion dies in the actual production. From this figure, the non-uniform material flow in the cross section of the profile is observed, and the material in both ends flows faster than that in the center. More importantly, after several rounds of extrusion production, cracks appear in the extrusion die due to stress concentration, and finally cause the fracture of the extrusion die. And the die crack occurs near the bearing land, which is coated with white paint (Fig. 6b). The above problems lead to low finished product rate and high production cost. Therefore, in the following, based on numerical simulation and optimization algorithm, the initial design of extrusion dies will be optimized to improve the material flow and reduce the stress concentration.

Table 1 Process parameters in actual extrusion production

Billet dimension (mm)	Ø304 × 820
Extrusion ratio	31.2
Initial temperature of billet (°C)	500
Initial temperature of die (°C)	480
Initial temperature of container (°C)	420
Extrusion velocity (mm/s)	1.88

2.2 Determination of material parameters of AA6N01

The 6N01 aluminum alloy is widely used in the extrusion process for producing the body profiles of high-speed trains. To provide accurate material parameters, its mechanics and thermo-physical parameters are examined by a series of experimental test, and the obtained material parameters are listed in Table 2.

In addition, the material parameter in the Arrhenius constitutive model with strain compensation is identified according to the stress-strain data obtained by hot compression tests of AA6N01 and then is applied to simulate the extrusion process of AA6N01:

$$\sigma = \frac{1}{c(\varepsilon)} \ln\left\{\frac{\dot{\varepsilon}\exp[e(\varepsilon)/RT]}{\exp[f(\varepsilon)]}\right\}^{\frac{1}{d(\varepsilon)}} + \left[\left(\frac{\dot{\varepsilon}\exp[e(\varepsilon)/RT]}{\exp[f(\varepsilon)]}\right)^{\frac{2}{d(\varepsilon)}} + 1\right]^{\frac{1}{2}} \quad (1)$$

where $c(\varepsilon)$, $d(\varepsilon)$, $e(\varepsilon)$, $f(\varepsilon)$ are the polynomial function of strain, which are used to represent the material constants (α, n, Q, A), respectively.

$$\begin{aligned} \beta &= B_0 + B_1\varepsilon + B_2\varepsilon^2 + B_3\varepsilon^3 + B_4\varepsilon^4 \\ a &= C_0 + C_1\varepsilon + C_2\varepsilon^2 + C_3\varepsilon^3 + C_4\varepsilon^4 \\ n &= D_0 + D_1\varepsilon + D_2\varepsilon^2 + D_3\varepsilon^3 + D_4\varepsilon^4 \\ Q &= E_0 + E_1\varepsilon + E_2\varepsilon^2 + E_3\varepsilon^3 + E_4\varepsilon^4 \\ \ln A &= F_0 + F_1\varepsilon + F_2\varepsilon^2 + F_3\varepsilon^3 + F_4\varepsilon^4 \end{aligned} \quad (2)$$

The values of polynomial fitting coefficient are listed in Table 3. The comparison between the measured flow stresses (corrected by temperature and friction error) and the predicted results is shown in Fig. 7. It can be seen that there are good agreements between the flow stresses obtained by two methods, especially at higher temperature. The process of establishing the Arrhenius constitutive model of AA6N01 used in this study has been completed in our previous research [19].

2.3 Modeling of the extrusion process

To simulate material flow and die strength during the extrusion process, a steady state finite element model is built based

(a) front-end of the profile (b) the damaged die with crack

Fig. 6 Front-end of the profile and the damaged die with crack

on HyperXtrude, which is composed of metal flow analysis model and die deformation and strength analysis model, as shown in Fig. 8.

The 6N01aluminum alloy and the H13 tool steel are chosen as the billet material and the die material, respectively. The process parameters used in numerical simulation are identical to those in extrusion experiment (Table 2). As a more dedicated aluminum alloy, there is no material data of AA6N01 in HyperXtrude's material library, so a user-defined model is developed by embedding above constitutive equation to describe hot deformation behavior during extrusion process. The user-defined material constitutive model is triggered in numerical simulation by a dynamic link library of UDF_MatModel.dll.

2.4 Analysis of simulation results and experiment verification

After simulation, the material flow velocity in the cross section of the profile is shown in Fig. 9. From the figure, it is seen that the material in the both ends flows slightly faster than that in the center. The maximum and minimum velocities of profile are 63.31 and 54.68 mm/s, separately, and the maximum velocity difference in the entire cross section is 8.63 mm/s, which agrees with the experimental front-end of the profile as observed in Fig. 6.

In order to investigate the potential causes of die fracture, the displacements and stresses of the extrusion die will be analyzed. In extrusion process, the deformation of die has a great influence on the outline of extrudate and is the main factor of extrudate error. The displacement distributions in the dies along X, Y, and Z directions during numerical simulations are shown in Fig. 10. It is seen that Z displacements on extrusion dies are relatively concentrated, which X displacements and Y displacements almost could be ignored. However, it is noticed that the Z displacements of the extrusion die have little influence on the dimension precision of the profile.

In actual extrusion production, extrusion dies always work with multicycles of loading-unloading at elevated temperature, so it is easy to generate plastic deformation or fracture, especially under the condition of severe stress concentration. The stress distributions on extrusion dies are shown in Fig. 11. The maximum stress of about 580 MPa on the spread die appears at the die exit, the maximum stress of about 795 MPa on the upper die is located on the part between bridges and mandrels, and the maximum stress of about 661 MPa on the lower die occurs near the part where the fracture was observed in the extrusion experiment. So, the comparison shows that the numerical results are in good agreement with experimental observations, which verifies the accuracy of the numerical model. But it needs to be declared that elastic deformation only happens on the extrusion dies according to the yield strength of H13 tool steel [20].

3 Structure optimization of the spread extrusion die

3.1 Definition of design variables and the response

The height (H), the width (B), and the maximum circumcircle diameter (L) at the entrance of the spread die have a great influence on the material flow along the spread direction. Therefore, in order to obtain more reasonable

Table 2 Material parameters of AA6N01 obtained by experimental test

Density (kg/m^3)	2700
Specific heat (J/(kg K))	947
Thermal conductivity (W/(m K))	195.7
Young's modulus (Pa)	3.53×10^{10}
Poisson's ratio	0.3
Average linear expansion coefficient (k^{-1})	2.83×10^{-5}

Table 3 Constants of the four polynomial fittings

α		n		Q		ln$A$	
C_0	0.029	D_0	11.160	E_0	367.568	F_0	55.545
C_1	−0.043	D_1	−36.636	E_1	−1,147.593	F_1	−174.441
C_2	0.201	D_2	166.205	E_2	5,395.428	F_2	826.665
C_3	−0.394	D_3	−376.270	E_3	−12,903.128	F_3	−1,988.263
C_4	0.312	D_4	322.990	E_4	11,660	F_4	1,801.811

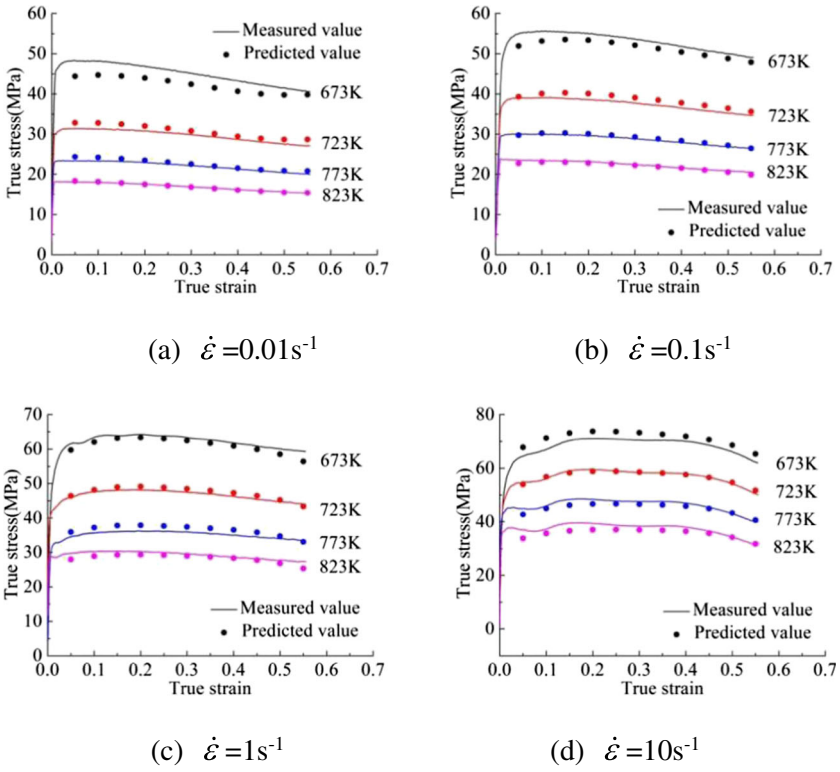

Fig. 7 Comparison of the rheological stress of prediction and experiment values

structure of the spread die, the three structural parameters are chosen as the design variables to be optimized, as shown in Fig. 12. The value ranges of design variables are listed in Table 4. To obtain the most uniform material

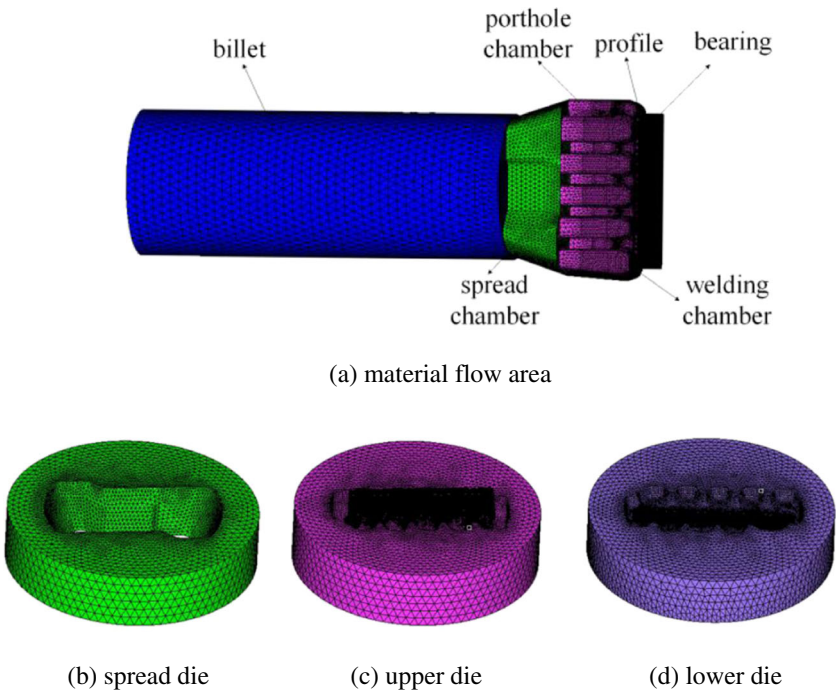

Fig. 8 Finite element model of aluminum alloy profile in simulation process

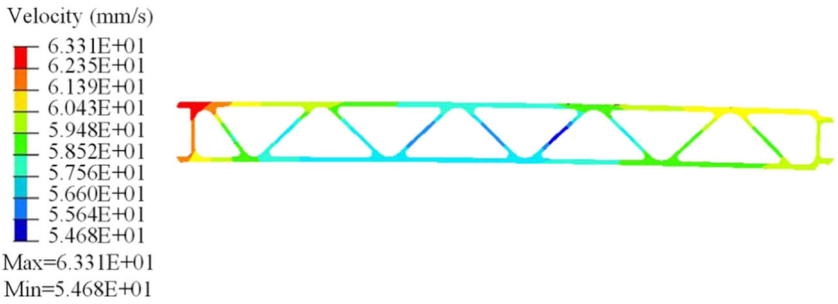

Fig. 9 Velocity distribution in the cross section of profile

flow in die cavity, the square deviation velocity (SDV) in the cross section of the profile at die exit is defined as the response to describe the velocity uniformity of the profile. SDV could be expressed as follows [8]:

$$\mathrm{SDV} = \sqrt{\frac{\sum_{i=1}^{n}\left(v_i - \overline{v}\right)^2}{n}} \tag{3}$$

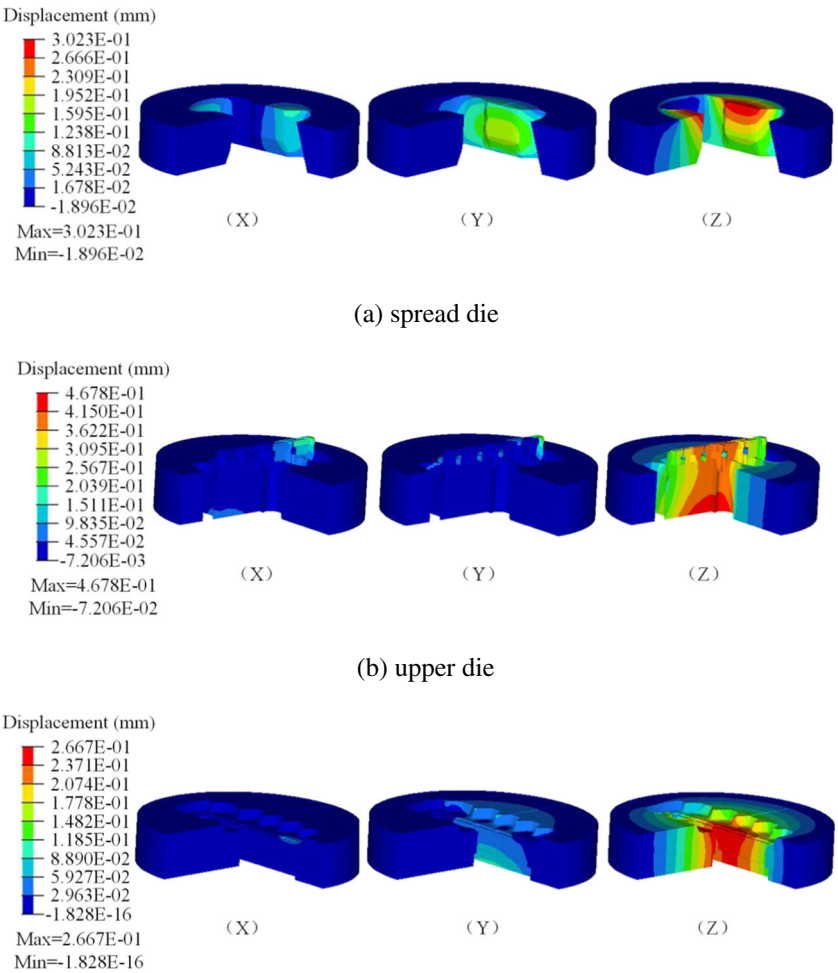

Fig. 10 Displacement distributions on the extrusion dies along *X*, *Y*, and *Z* directions

(a) spread die

(b) upper die

(c) lower die

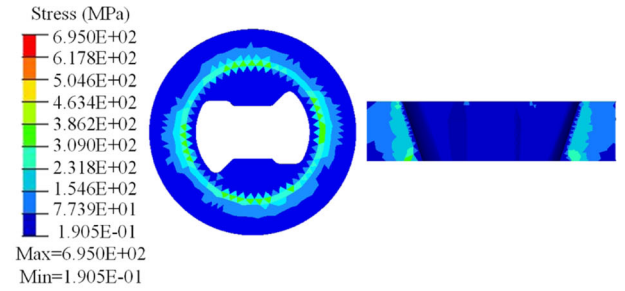

(a) spread die

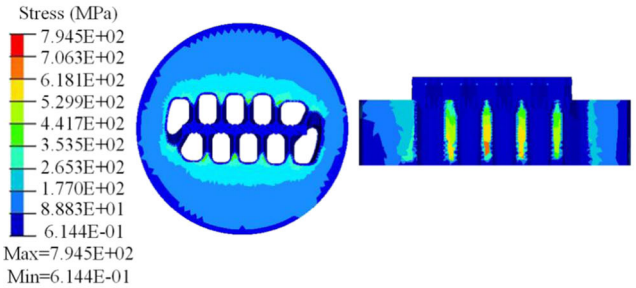

(b) upper die

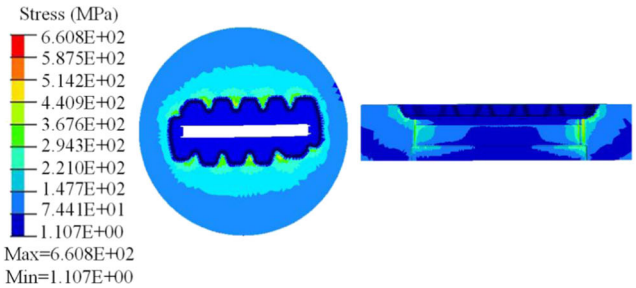

(c) lower die

Fig. 11 Stress distributions on the extrusion dies

where v_i is the flow velocity of node i at the exit section of the profile, $\bar{v}$ is the average speed of all nodes on the profile exit section, and n is the total number of nodes on the exit section.

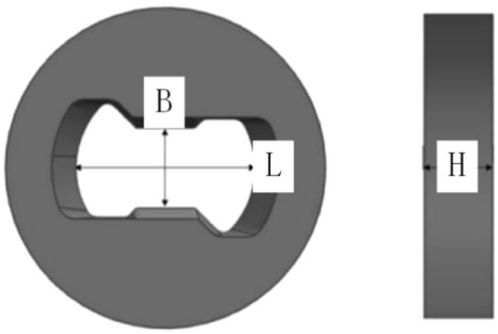

Fig. 12 Definition of design variables of the spread die

Table 4 Value ranges of design variables

Design variables	Range (mm)
H	80–140
B	60–80
L	290–300

3.2 Design of experiments with Box-Behnken method

Design of experiments (DOEs) with Box-Behnken method are used, and 17 combinations of three design variables are obtained, as listed in Table 5. Then, corresponding numerical models are built and steady state numerical simulations are carried out. The SDV in the cross section of the profile at die exit is finally calculated for each experiment design.

3.3 Fitting and analysis

Based on the data in Table 5, a response surface function between the response and design variables is obtained by the following least squares fitting:

$$\begin{aligned} \mathrm{SDV} = {} & 1.25 - 1.68 \times H + 1.22 \times B - 0.37 \\ & \times L - 1.42 \times H \times B + 0.53 \times H \times L - \\ & 0.47 \times B \times L + 1.09 \times H^2 + 0.75 \times B^2 \\ & + 0.38 \times L^2 \end{aligned} \tag{4}$$

Table 5 Design of experiments and calculated SDV

Combination no.	Design of experiment			SDV (mm/s)
	H (mm)	B (mm)	L (mm)	
1	80	80	295	7.49
2	140	60	295	1.55
3	110	80	290	4.14
4	80	70	290	5.1
5	140	70	290	0.92
6	110	60	300	1.56
7	110	60	290	1.12
8	80	70	300	3.48
9	110	70	295	1.25
10	140	80	295	1.48
11	80	60	295	1.87
12	140	70	300	1.00
13	110	70	295	1.25
14	110	80	300	2.71
15	110	70	295	1.25
16	110	70	295	1.25
17	110	70	295	1.25

Table 6 Variance analysis and significance test of the SDV

Source	Sum of squares	Free degree	Mean square	*F* value	*P* value
Model	54.25	9	6.03	100.97	<0.0001
A	22.46	1	22.46	376.22	<0.0001
B	11.83	1	11.83	198.20	<0.0001
C	1.08	1	1.08	18.11	0.0038
AB	8.09	1	8.09	135.50	<0.0001
AC	1.11	1	1.11	18.60	0.0035
BC	0.87	1	0.87	14.63	0.0065
A^2	5.04	1	5.04	84.48	<0.0001
B^2	2.38	1	2.38	39.79	0.0004
C^2	0.62	1	0.62	10.39	0.0146
Residual	0.42	7	0.060		
Lack of fit	0.42	3	0.14		
Pure error	0.000	4	0.000		
Correlation total	54.67	16			
R-squared = 0.992			Adjusted *R*-squared = 0.983		
Predicted *R*-square = 0.878			Adequate precision = 34.777		

According to above function, the SDV of the profile in the cross section at die exit can be calculated for different combinations of design variables.

In order to evaluate the reliability of the response surface model, the variance analysis and the significance test of the model are carried out, as listed in Table 6. *P* value is less than 0.05 for this model; it indicates that the response surface function in Eq. (4) has an obvious and significant influence on the response results. *R*-squared is 0.992, which indicates that the function model given in Eq. (4) has a good model fitting and a small error. Therefore, the function model can be used. The adjusted *R*-squared is 0.983, which means that this model can explain 98.3% of the response results, and only 1.7% of the response results cannot be explained. The adequate precision is 34.777 and larger than 4, which shows that the precision is good enough. The above analysis shows that the model given by Eq. (4) is suitable for analyzing and predicting the objective function SDV.

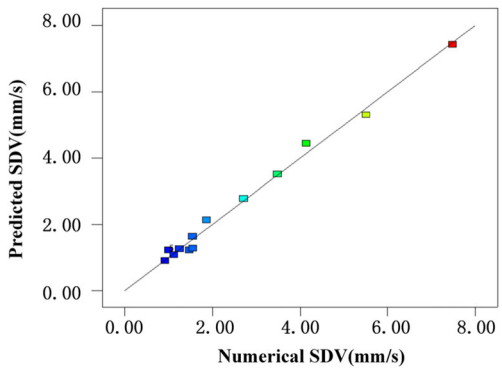

Fig. 13 Comparison between the numerical and predicted SDVs

The comparison between the numerical and predicted SDVs is shown in Fig. 13. It is shown that the predicted SDVs are basically identical to the numerical ones, so the regression model can accurately predict the result.

The response plots of SDV in terms of design variables are shown in Fig. 14. Figure 14a gives the relationship between SDV and design variables *B* and *H*, while the design variable *L* is 295 mm. It shows that the SDV firstly decreases and then increases with the increase of *B* when *H* is larger than 120 mm. This indicates that for each value *H*, there is a certain value of *B* to get better control of material flow and a better value of SDV. When *H* is less than 120 mm, there is a small distance for material flow in the spread die cavity. For this case of small height, it is too difficult to adjust the material flow timely. In this moment, the SDV is increased with the increase of *B*. Figure 14b gives the relationship between SDV and the design variables *L* and *H*, while the width *B* at the center of the entrance is 70 mm. It is seen that the SDV decreases firstly and then slowly increases with the increase of *H*. Figure 14c gives the relationship between SDV and the design variables *L* and *B*, which the height *H* is 110 mm. It is indicated that the SDV has little change with the increase of *L* when *B* is less than 70 mm.

3.4 Optimization and validation of response surface

To obtain the most uniform material flow, the minimum SDV is calculated as 0.59 mm/s according to Eq. (4). To verify above optimization result, a corresponding finite element model with the optimal design variables is built and the

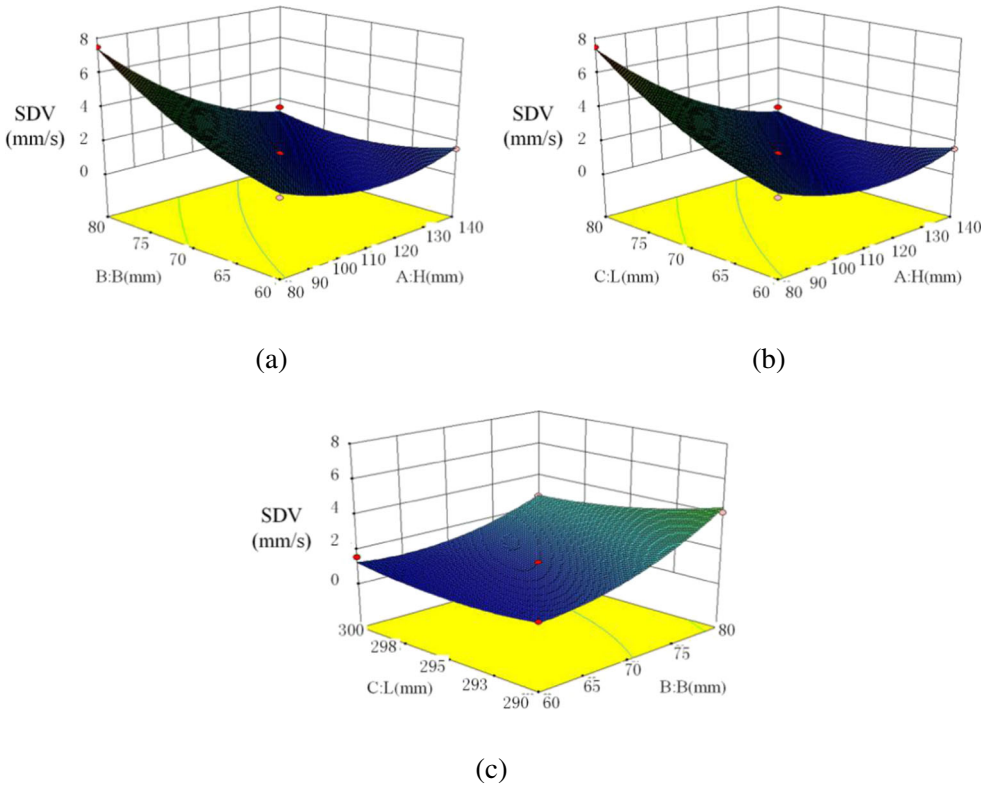

Fig. 14 Response surface of SDV in terms of design variables

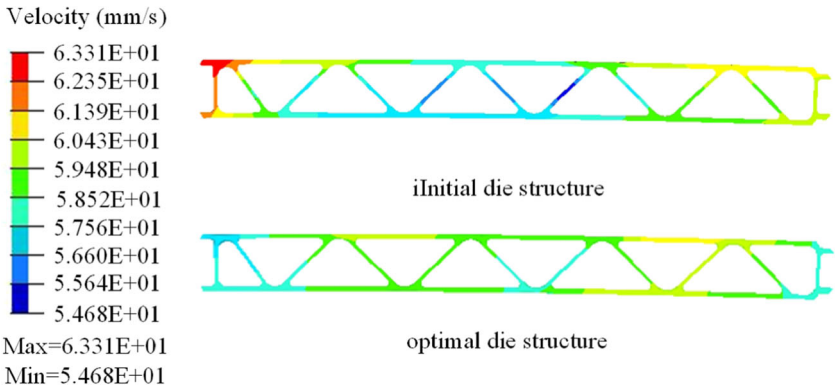

Fig. 15 Velocity distribution of the profile for the initial and optimal die structures

Table 7 Comparison of the spread die structure parameters and material flow

	Before optimization	After optimization
H	120	129
B	67	68
L	300	294
Maximum velocity difference	8.63	3.07
SDV	1.56	0.69

extrusion process is simulated. After simulation, the SDV in the cross section of the profile at die exit is 0.69 mm/s according to Eq. (3), which is similar with the predicted one. The comparison of velocity distribution with the initial and optimal dies is shown in Fig. 15. It is seen that the maximum velocity difference in the entire cross section drastically decreases. The comparison of the structure and material flow parameters with the initial and optimal dies is listed in Table 7. The maximum velocity difference decreases from 8.63 to 3.07 mm/s, and the corresponding SDV decreases from 1.56 to 0.69 mm/s. So, after optimization, the material flow distribution tends to be more uniform.

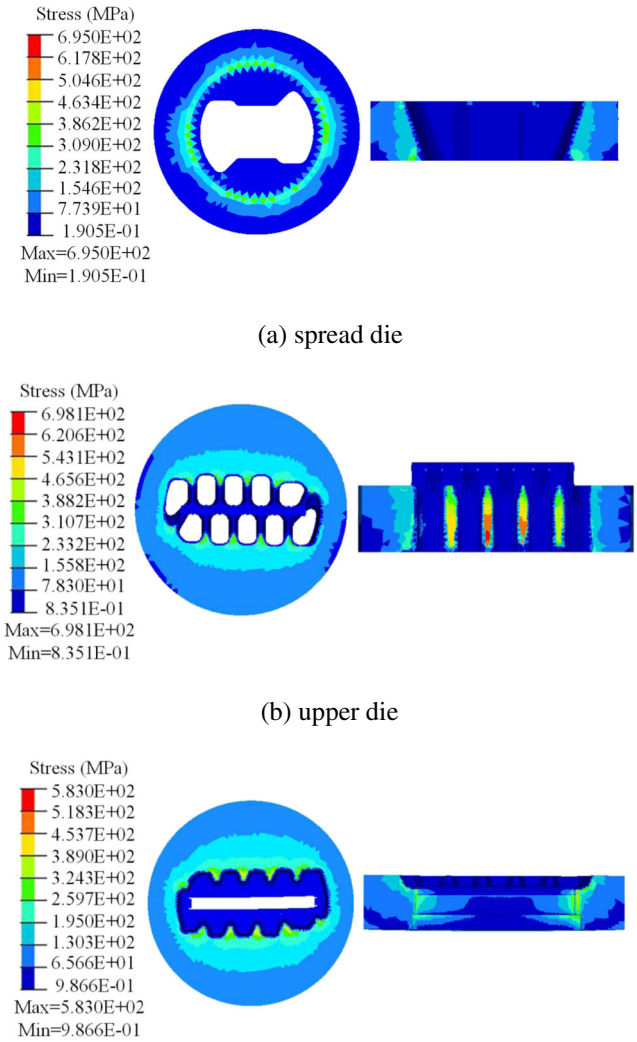

(a) spread die

(b) upper die

(c) lower die

Fig. 16 Stress distributions on extrusion dies after optimization

The stress distributions on extrusion dies after optimization are shown in Fig. 16. Compared with Fig. 11, the maximum stress in the spread die increases, while the maximum stresses in the upper and lower dies decrease.

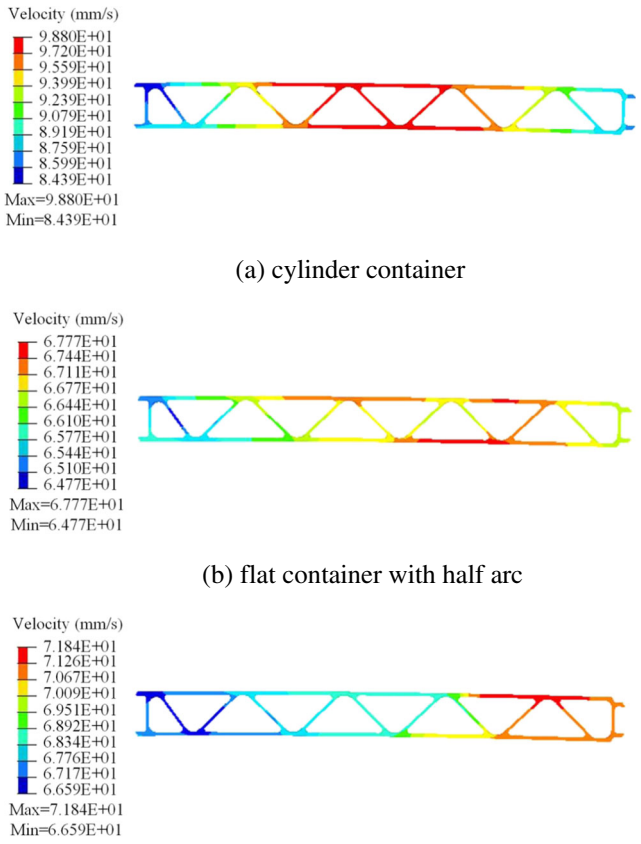

(a) cylinder container

(b) flat container with half arc

(c) flat container with elliptic arc

Fig. 18 Velocity distributions of the profile with cylinder and flat containers

4 Application of flat containers in extrusion process

4.1 Comparative design of flat containers

The inner hole of flat container is usually designed as the rectangle shape with arc surface edges. The ratio of width to height of the inner hole is best between 2 and 3 [21]. The extrusion coefficient, the width of the extrudate, and the property of the selected light alloy have a great influence

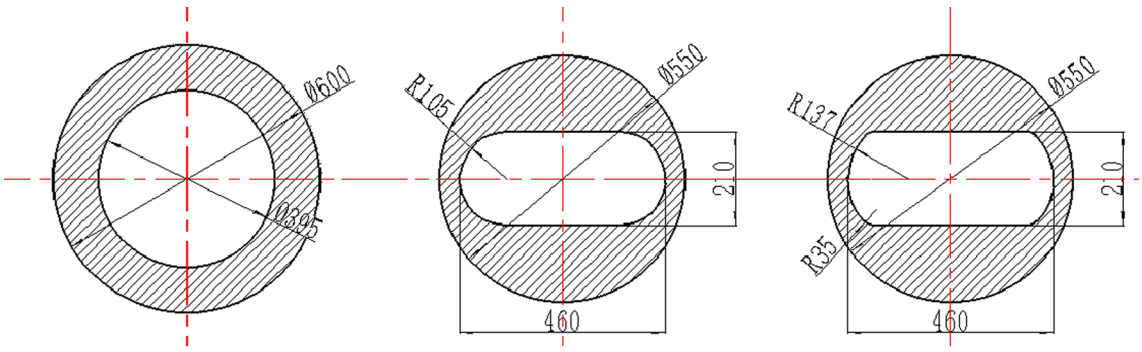

(a) cylinder container (b) flat container with half arc (c) flat container with elliptic arc

Fig. 17 Inner hole shape of different extrusion containers

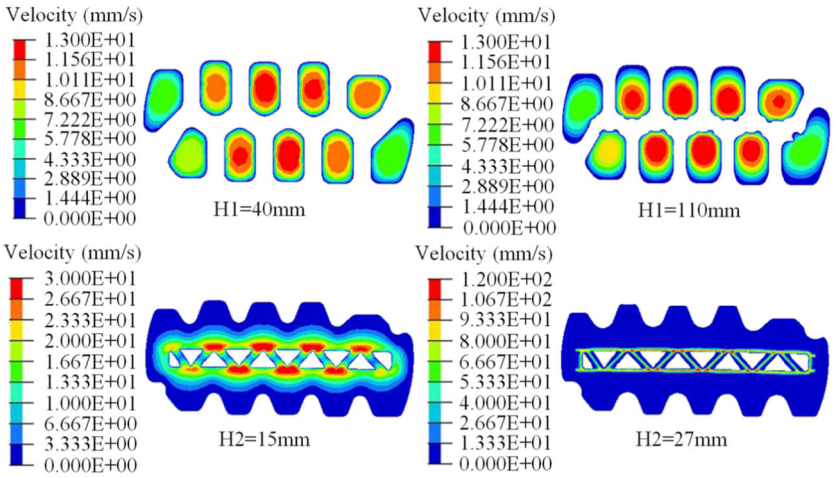

(a) cylinder container

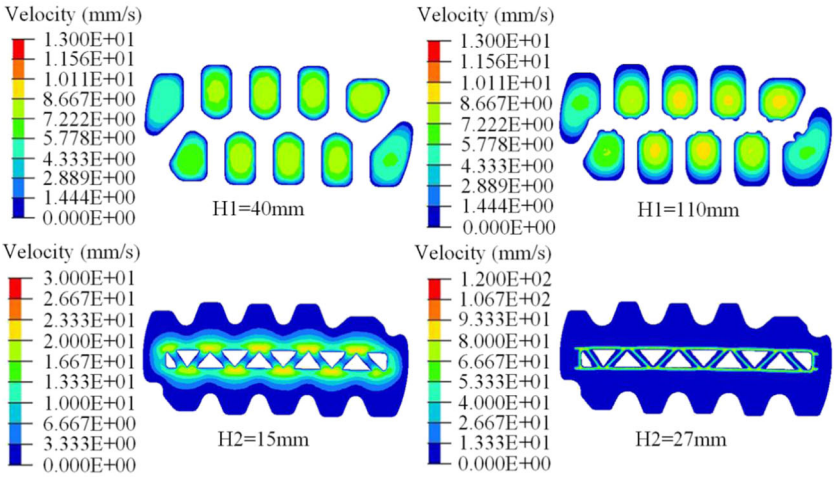

(b) flat container with half arc

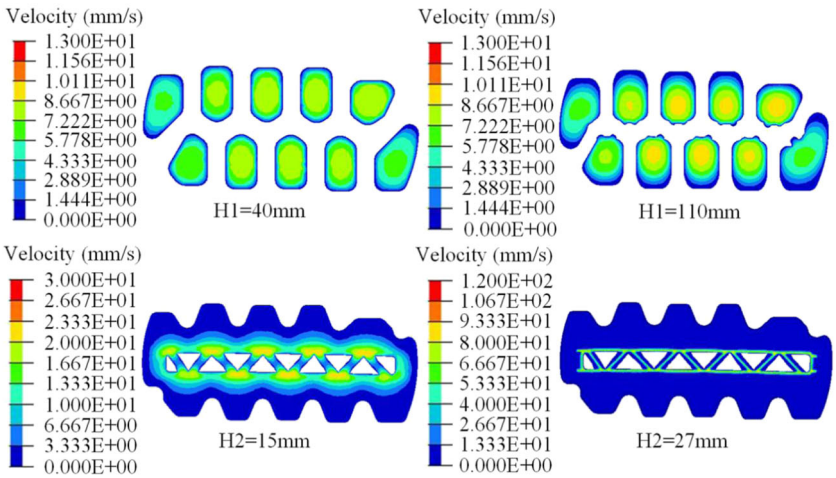

(c) flat container with elliptic arc

Fig. 19 Flow velocity distributions at different extrusion stages with cylinder and flat containers

on the size of inner hole. The ratio of inner hole's width to outer diameter of container is best controlled in the range from 0.8 to 0.9, and once it goes beyond this range, the strength of container cannot be ensured [21]. The pore size

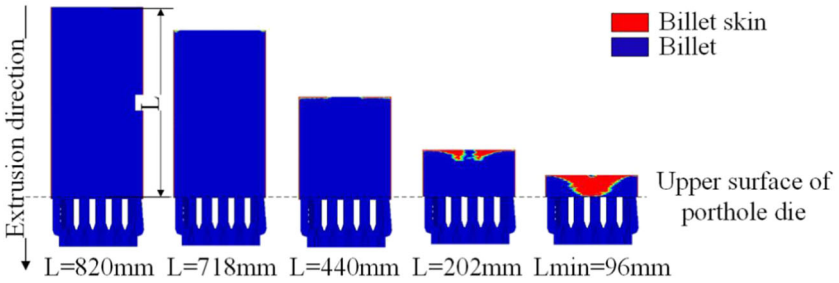

(a) cylinder container

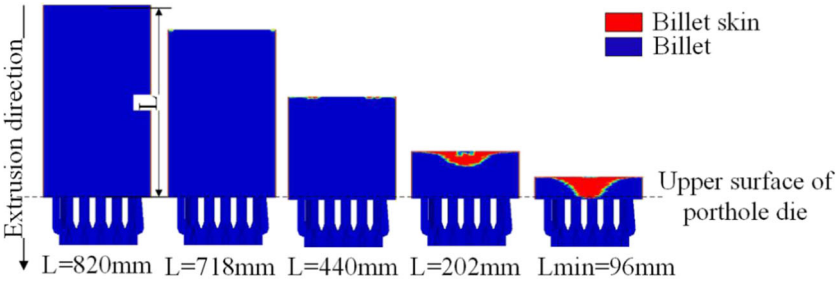

(b) flat container with half arc

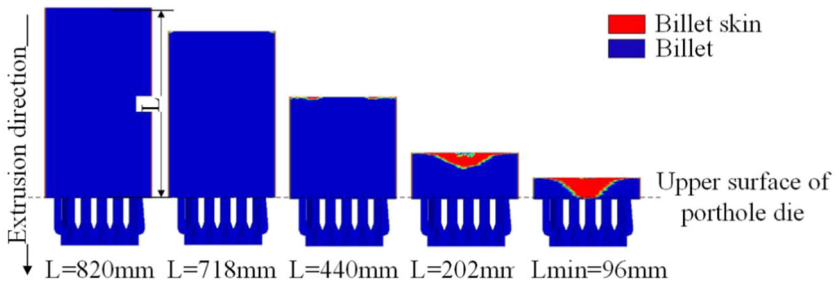

(c) flat container with elliptic arc

Fig. 20 Comparison of the billet skin during different extrusion containers

of container, the property of the selected light alloy, the structure of the extrusion press, and the strength of the ram have effect on the length of container. Especially to the flat container, the larger length of container easily leads to the bending deformation of the ram.

In this work, combing the design specification of the light alloy extrusion tool and the actual production, two different transition forms of flat containers are designed, comparatively. Their inner hole sizes are both 460 × 210 mm. Its outside diameter and length sizes are 550 and 1230 mm, respectively. So, the ratio of width to height of the inner hole and inner hole's width to outer diameter of container are 2.2 and 0.84, respectively, and which meet the standard. In order to facilitate comparison, another cylinder container is also designed. And its inner hole diameter and the outside diameter are 395 and 600 mm, respectively, as shown in Fig. 17.

Here, the same upper and lower dies are used in the flat and cylinder container extrusion processes, as shown in Fig. 4b, c, but the spread die is not used.

4.2 Modeling and analysis of extrusion process with flat container

4.2.1 Analysis of material flow

The velocity distributions in the cross section of the profile with different extrusion containers are shown in Fig. 18. It is seen that the material flow velocity of profile is very non-uniform with the cylinder container. And it flows much faster in the center than that in both ends. The maximum and minimum velocities of profile are 98.8 and 84.39 mm/s, respectively, and the maximum velocity difference in the entire cross section is 14.41 mm/s. Compared with the cylinder container,

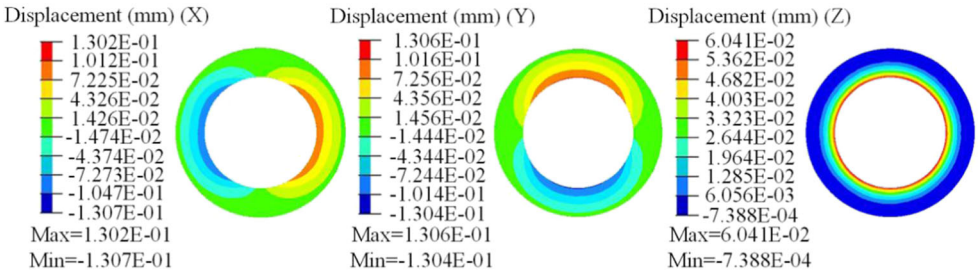

(a) cylinder container

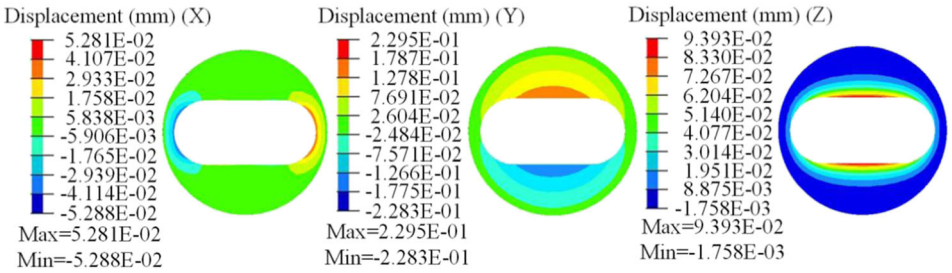

(b) flat container with half arc

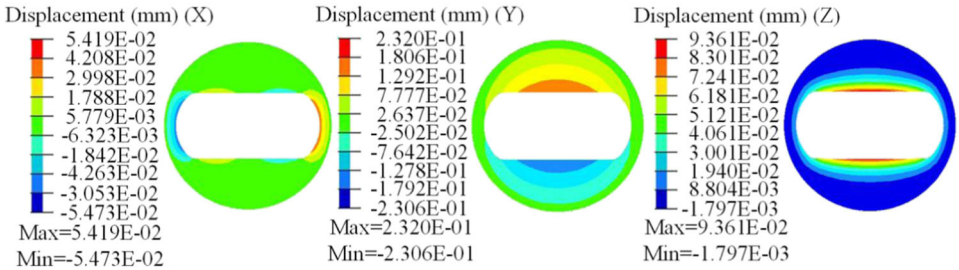

(c) flat container with elliptic arc

Fig. 21 Displacements on different extrusion containers

due to the cross-section similarity of the inner hole of flat containers with the shape of the profile, the overall material velocity distribution is improved effectively. The material flow velocity becomes uniform with the flat containers, and the maximum velocity differences in the entire cross section are only 3 and 5.25 mm/s, respectively. However, it is seen that the average flow velocity is always larger with cylinder container than that with flat containers due to different extrusion ratios.

The material flow distributions during different extrusion stages with different extrusion containers are shown in Fig. 19. Compared with flat containers, the material velocity difference with cylinder container is always large during entire extrusion process, especially in the final stage of the extrusion.

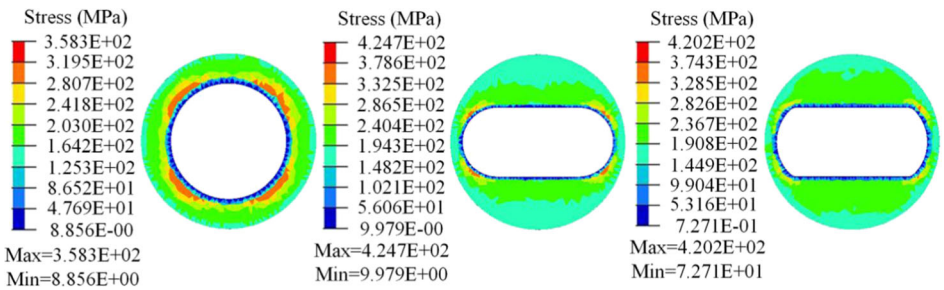

(a) cylinder container (b) flat container with half arc (c) flat container with elliptic arc

Fig. 22 Stress distributions on different extrusion containers

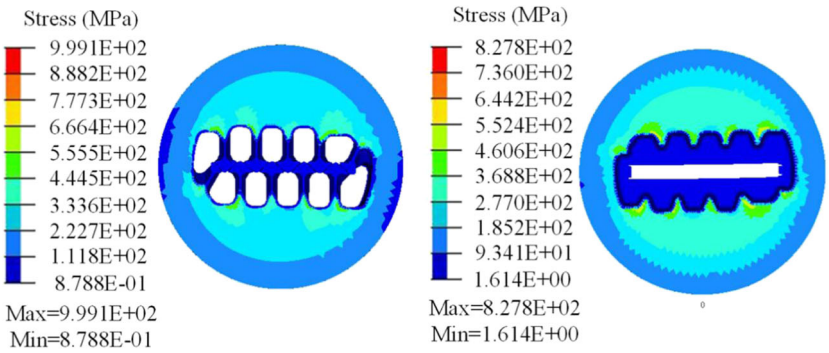

(a) cylinder container

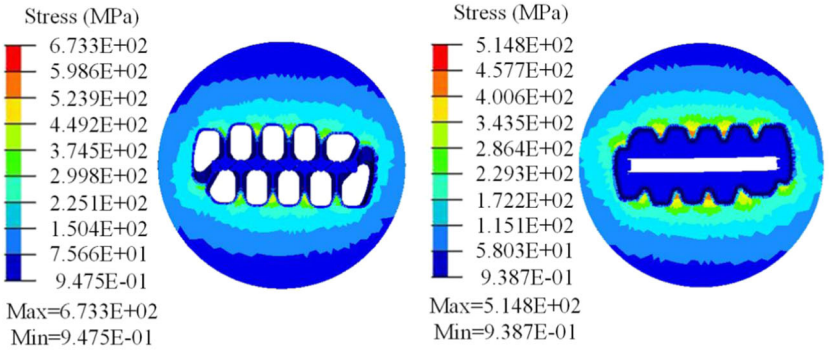

(b) flat container with half arc

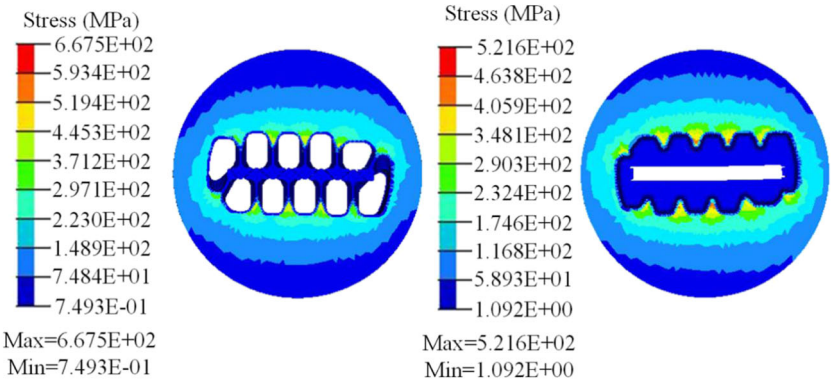

(c) flat container with elliptic arc

Fig. 23 Stress distributions on the extrusion dies with cylinder and flat containers

4.2.2 Analysis of the billet skin

The flow behaviors of the billet skin at different times with different extrusion containers are shown in Fig. 20. It shows that at the early stage of extrusion, for the frictions from the container, the skin of the billet flows slower than the ram velocity, then is accumulated around the corner between the container wall and the ram, and flows from the edge to the center along the ram surface. The lengths of the billet skin in the flat containers are longer than that in the cylinder container at this time, and the length difference is small for different transition forms of the flat containers. As the extrusion process goes, the billet skin sequentially flows along the extrusion direction until it reaches the entrance of upper die. At the moment, the lengths of the billet skin in different extrusion containers are the same, with 11.7% of the total length of initial billet. So the change of the inner hole shape of container has little effect on the butt length and the material utilization.

4.2.3 Analysis of the displacement and stress on extrusion die

The comparison of the displacements on the extrusion containers along the *X*, *Y*, and *Z* directions is shown in Fig. 21. It is shown that *X* displacement and *Y* displacement are greater than *Z* displacement, and *X* displacement and *Y* displacement are on the same order of magnitude on the cylinder container.

However, due to its geometrical asymmetry of the flat containers, Y displacement is significantly larger than X displacement.

The stress distributions on extrusion containers are shown in Fig. 22. It is seen that the maximum stress on cylinder container is distributed more uniformly than that on flat container, and the former is about lower 65 MPa than the latter.

Due to the uniform material flow in the flat container extrusion, the stresses on upper and lower dies are significantly lower than those in cylinder container extrusion, as shown in Fig. 23.

5 Conclusions

In this work, the recently developed spread die and flat container extrusions were applied for a large, hollow, and flat-wide aluminum alloy profile used in high-speed train and the extrusion numerical simulation processes were analyzed. The following conclusions were drawn:

(1) A thermo-mechanical model was established to analyze the extrusion process of a complex-section aluminum alloy profile. Then, numerical simulation results were compared with the experimental observations and verified well. More importantly, it was shown that a spread die could effectively improve the material supply in spread direction.
(2) The optimization of the spread extrusion die was carried out by combining design of experiments with response surface method. After optimization, the material flow distribution was more uniform than before optimization. The maximum velocity difference in the cross section of the profile reduced from 8.63 to 3.07 mm/s, and the corresponding SDV reduced from 1.56 to 0.69 mm/s.
(3) The flat container extrusion was simulated compared with traditional cylinder container extrusion. The material flow uniformity during the flat container extrusion could be greatly improved. The maximum velocity difference decreased from 14.41 to 3 mm/s. Meanwhile, the maximum stress on the extrusion dies reduced from 999 to 670 MPa, and the dead zone also greatly decreased. However, the displacements on flat containers were more non-uniform, and its maximum stress was higher about 65 MPa than that on the cylinder container.
(4) Compared with the flat container with elliptic arc, the material flow velocity distribution in the flat container with half arc was more uniform; the maximum velocity difference decreased from 5.25 to 3 mm/s. However, the inner hole shape of the flat container had little effect on the dead zone, butt length, container displacement, and extrusion tool stress in extrusion numerical simulation process.

Acknowledgements The authors would like to acknowledge financial support from National Natural Science Foundation of China (51575315), Fund of Science and Technology Development of Guangdong Province (2017A010103003), Key Research and Development Program of Shandong Province (2017GGX30140), and Fundamental Research Funds of Shandong University (2015WLJH29).

References

1. Lee JM, Kim BM, Kang CG (2005) Effects of chamber shapes of porthole die on elastic deformation and extrusion process in condenser tube extrusion. Mater Des 26(4):327–336
2. Yang DY, Park K, Kang YS (2001) Integrated finite element simulation for the hot extrusion of complicated Al alloy profiles. J Mater Process Technol 111:25–30
3. Liu P, Xie SS, Cheng L (2012) Die structure optimization for a large, multi-cavity aluminum profile using numerical simulation and experiments. Mater Des 36:152–160
4. Zhao GQ, Chen H, Zhang CS, Guan YJ, Gao AJ, Li P (2014) Die optimization design and experimental study of a large wallboard aluminum alloy profile used for high-speed train. Int J Adv Manuf Technol 74(1–4):539–549
5. Zhang CS, Zhao GQ, Guan YJ, Gao AJ, Wang LJ, Li P (2015) Virtual tryout and optimization of the extrusion die for an aluminum profile with complex cross-sections. Int J Adv Manuf Technol 78(5):927–937
6. Sun XM, Zhao GQ, Zhang CS, Guan YJ, Gao AJ (2013) Optimal design of second-step welding chamber for a condenser tube extrusion die based on the response surface method and the genetic algorithm. Mater Manuf Process 28(7):1872–1878
7. Reddy M, Mayavaram R, Durocher D, Carlsson H, Bergquist O (2004) Analysis and design optimization of aluminum extrusion dies. Proc Eight Int Alum Extrusion Technol Semin 1: 231–235
8. Zhang CS, Yang S, Zhang QY, Zhao GQ, Liu P (2017) Automatic optimization design of a feeder extrusion die with response surface methodology and mesh deformation technique. Int J Adv Manuf Technol 91:3181–3193
9. Mayavaram R, Sajja U, Secli C, Niranjan S (2013) Optimization of bearing lengths in aluminum extrusion dies. Procedia Cirp 12(12): 276–281
10. Bje RV (1999) Finite element simulation of the aluminum extrusion process: shape prediction for complex profiles. J Antibiot 53(1):33–37
11. Sajko N, Kovacic S, Balic J (2013) Simulation based CAD/CAM model for extrusion tools. Adv Prod Eng Manag 8(1):33–40
12. Abrinia K, Makaremi M (2009) An analytical solution for the spread extrusion of shaped sections. Int J Adv Manuf Technol 41(7):670–676
13. K. Abrinia, M. Makaremi (2007) An upper bound solution for the spread extrusion of elliptical sections, AIP Conf Proc 907(1): 614–619
14. Lesniak D, Libura W (2007) Extrusion of sections with varying thickness through pocket dies. J Mater Process Technol 194(1): 38–45
15. Fang G, Zhou J, Duszczyk J (2008) Effect of pocket design on metal flow through single-bearing extrusion dies to produce a thin-walled aluminium profile. J Mater Process Technol 199(1–3): 91–101
16. Xu ZY, Wang Y, Dong PL, Xiao K (2008) Shrinkage optimization of flat receptacle using the finite element method. Mater Sci Forum 575-578:478–482

17. L.H. Duan (2012) The deformation analysis and structural optimization of the inner hole of container. Dissertation, Chongqing University
18. J. Wang (2003) Strength analysis and design methods of the flat container. Dissertation, Yanshan University
19. Dong YY, Zhang CS, Zhao GQ, Guan YJ, Gao AJ (2015) Constitutive equation and processing maps of an Al-Mg-Si aluminum alloy: determination and application in simulating extrusion process of complex profiles. Mater Des 92:983–997
20. G.R. Speich (2005) Dual Phase Steel, ASM Handbook Vol 1: Properties and Selection: Irons, Steels and High Performance Alloys section, ASM International:697–707
21. Zhao XL, Xue LJ, Liu JA (2005) Design of the flat extrusion cylinder. Forging & Stamping Technol 30:87–94